Metabasic Rocks as Important Nitrogen Carriers to Forearc Depths: Implications for Deep Nitrogen Cycling

Ananya Mallik, Anna M Rebaza, Paul Kapp, Long Li, Yifan Du, Ahmed Al Shams, Emily H. G Cooperdock

PII: S0016-7037(23)00481-7

DOI: https://doi.org/10.1016/j.gca.2023.10.007

Reference: GCA 13187

To appear in: Geochimica et Cosmochimica Acta

Received Date: 14 June 2023

Revised Date: 28 September 2023 Accepted Date: 2 October 2023



Please cite this article as: Mallik, A., Rebaza, A.M., Kapp, P., Li, L., Du, Y., Al Shams, A., H. G Cooperdock, E., Metabasic Rocks as Important Nitrogen Carriers to Forearc Depths: Implications for Deep Nitrogen Cycling, *Geochimica et Cosmochimica Acta* (2023), doi: https://doi.org/10.1016/j.gca.2023.10.007

This is a PDF file of an article that has undergone enhancements after acceptance, such as the addition of a cover page and metadata, and formatting for readability, but it is not yet the definitive version of record. This version will undergo additional copyediting, typesetting and review before it is published in its final form, but we are providing this version to give early visibility of the article. Please note that, during the production process, errors may be discovered which could affect the content, and all legal disclaimers that apply to the journal pertain.

© 2023 Published by Elsevier Ltd.

Metabasic Rocks as Important Nitrogen Carriers to Forearc Depths: Implications for Deep Nitrogen Cycling

Ananya Mallik^{a*}, Anna M Rebaza^a, Paul Kapp^a, Long Li^b, Yifan Du^b, Ahmed Al Shams^a, Emily H. G Cooperdock^c

^aDepartment of Geosciences, University of Arizona, 1040 E 4th St., Tucson, AZ 85715, USA

^bDepartment of Earth & Atmospheric Sciences, University of Alberta, Edmonton, Alberta, T6G 2E3, Canada

^cDepartment of Earth, Environmental and Planetary Sciences, Brown University, Box 1846, 324 Brook Street, Providence, RI 02912, USA

* Corresponding author, email: mallika@arizona.edu

Abstract

Understanding deep nitrogen (N) cycling better requires investigating the delivery of N to subduction systems via various lithologies. Input to subduction zones through mafic rocks is more voluminous and massive as compared to sedimentary rocks which calls for a thorough investigation of the behavior of N in metabasic rocks. Here we estimate

the delivery of N to subduction zones at fore-arc depths by investigating the geochemistry of amphibolites and epidote-blueschists from the Central Qiangtang Metamorphic Belt in Tibet where the metabasic rocks likely represent the transition from oceanic to continental subduction. The rocks contain 21-147 ppm N with δ^{15} N values from +1.8% to +10.0%, and 147 ppm N is the highest that has been reported in a metabasic rock thus far. Given the N abundances for most of the rocks are much higher than those of altered oceanic crust (i.e. basalts, sheeted dikes and gabbros; 6.0 ± 4.7 ppm), the N is likely neither magmatic nor was introduced in the rocks during hydrothermal alteration prior to subduction. This is confirmed by the K₂O/Th versus Ba/Th, Th/U versus Th and Ba/Rb versus K₂O plots where these rocks align with the trend of metamorphic fluid alteration rather than seafloor hydrothermal alteration. A twostep process led to N acquisition in the metabasic rocks. In the first step, the metabasic rocks acquired their N from metasediment-derived fluids during metamorphism in the subduction channel. In the second step, some of the metabasic rocks underwent N loss and concomitant enrichment in ¹⁵N due to devolatilization within the subduction channel. We modeled the N fluxes at fore-arc depths in 55 modern-day subduction zones via metasedimentary and metabasic rocks assuming their minimum, median and maximum N concentrations to assess their relative importance in delivery of N to subduction zones. We find that metabasic rocks supply comparable fluxes of N at forearc depths to metasedimentary rocks, even though metasedimentary rocks have at least an order of magnitude higher N abundance than metabasic rocks. This reinforces the need to investigate the behavior of N in metabasic rocks from more locations globally to improve our understanding of deep N cycling.

1. Introduction

Understanding the behavior of nitrogen (N) in subduction zones is an essential part of deep N cycling. The inputs of N to subduction zones take place via both continental and oceanic subduction and include a suite of lithologies such as continental and marine sediments, altered oceanic crust (AOC), dikes and sills emplaced on continents and abyssal serpentinites. At fore-arc depths and deeper, N delivery takes place via fore-arc processed mélanges that include metasedimentary, metabasic rocks and serpentinized lithosphere (e.g. Bebout and Barton, 2002; King et al., 2003; Cooperdock et al., 2018). To better constrain the delivery of N at fore-arc depths through these lithologies, it is important to assess their N concentrations and the factors which govern the distribution of N in these lithologies.

Metasediments have an order of magnitude higher median concentration of N (360 ppm for n = 155, based on data from Bebout and Fogel, 1992; Bebout, 1997; Busigny et al., 2003, 2005; Sadofsky and Bebout, 2003; Halama et al., 2010; Bebout et al., 2013; Cannaò et al., 2020) as compared to metabasic rocks (10 ppm for n = 118, based on the data from Halama et al., 2010, 2017; Busigny et al., 2011, 2018; K. Li et al., 2021; this study). This implies that sediments, after dehydration and metamorphism in the

accretionary prism or as they enter the subduction channel, retain a higher concentration of N as compared to metamorphosed mafic rocks (e.g. oceanic crust) undergoing the same processes. However, mafic input to subduction zones (mostly in the form of oceanic crust) is more voluminous than sediments which may lead to metabasic rocks being more effective in carrying N to forearcs and further depths than metasedimentary rocks (K. Li et al., 2021). Therefore, this calls for a thorough investigation of the behavior of N in metabasic rocks.

Previous studies have investigated N behavior in metabasic rocks to understand the processes through which N is acquired by the rock and the behavior of N during metamorphism. Halama et al. (2010) reported 2-20 ppm N (δ^{15} N = -1% to +8%) in eclogites from the Raspas Complex in Ecuador, Zambezi Belt in Zambia, Lago di Cignana in Italy and Cabo Ortegal in Spain. These eclogites had a range of N characteristics including a few that were nearly identical to altered oceanic crust (AOC), a few that had undergone effects of devolatilization, as well as a few that had metasomatic additions during subduction-zone metamorphism. In addition, Halama et al. (2017) measured N contents and isotope compositions ($\delta^{15}N = +1.0\%$ to +5.4%) in the blueschists and eclogites from Tianshan, China and observed a systematic decrease in N concentrations from blueschist (~26 ppm), to blueschist-eclogite transition zone (19-23 ppm) to eclogite (12-16 ppm) which they interpreted as a product of batch devolatilization process during metamorphism. Harris et al., (2022) reported the first in-situ measurements of N concentrations in phengite and chlorite within blueschists and eclogites from Lago di Cignana in Italy, Raspas Complex in Ecuador and Franciscan Complex in north-west California. They found that, while phengite is the principal host of N, chlorite has variable N abundance and maybe one of the key players in N cycling via metabasic rocks. The study also demonstrated the complexity in the mobility of N during subduction with not only fluid-rock interactions but redistribution of N between minerals (such as between phengite and pargasite) being important. Busigny et al. (2011, 2018) analyzed N concentrations (2.6 – 55 ppm) and isotope compositions ($\delta^{15}N = +0.8\%$ to +8.1%) in the metagabbros from the Western Alps such as greenschists and amphibolites from the Chenaillet Massif in France, blueschists from the Queyras region in France and eclogites from the Monviso Massif in Italy. Using Cu concentrations and δ^{65} Cu as tracers, they inferred that N was leached out from those metabasic rocks during hydrothermal alteration although this interpretation has been challenged by L. Li et al., (2021a). Finally, K. Li et al. (2021) reported the N abundances (14 - 122 ppm) and isotope compositions ($\delta^{15}N = -10.9\%$ to +3.7%) in the blueschists from the Heilongjiang Complex in Northeastern China. These blueschists were inferred to have altered oceanic crust as protoliths based on their preserved pillow textures. This is the first study that reported N concentrations >100 ppm in metabasic rocks and based on the N concentrations being higher than that in AOC, they inferred that N released from metasediments during metamorphism was refixed by metabasic rocks in a mélange zone. In summary, previous studies that have analyzed metabasic rocks for N inferred more than one process of N incorporation ranging from inheritance due to hydrothermal alteration at the seafloor, to hydrothermal leaching or devolatilization

during metamorphism, to addition of N during metamorphism in the subduction channel. Depending on the process, the N abundances and isotopic signatures vary widely across metabasic rocks from the regions mentioned above and thus the delivery of N to subduction zones can vary widely. This calls for further investigation of N characteristics in metabasic rocks from other regions to expand the database of N delivery by metabasic rocks and especially assess if one or more processes of N acquisition as inferred by the previous studies represent specific-case scenarios or are generally representative of subduction zones globally.

Nitrogen characteristics (abundance and isotopes) in metabasic rocks depend on (a) the formation conditions of the protoliths and (b) the processes that lead to N inheritance in the metabasic rocks. In this study, we investigate the supply of N to subduction zones by focusing on their delivery by metabasic rocks (amphibolites and epidote-blueschists) from the Central Qiantang Metamorphic Belt (CQMB) in Tibet where the mafic protoliths are seafloor basalts and seamounts (Zhai et al., 2011; Dan et al., 2019) although the metabasic rocks representing mafic sills and volcanics on continental margins cannot be precluded based on their interlayering with upper Paleozoic continental margin clastic and carbonate strata of the Qiangtang terrane (Kapp et al., 2003, Tang and Zhang, 2014). We analyze N abundances and isotope compositions, as well as trace elements in the samples to understand the process of N acquisition. We use N abundances for metasedimentary and metabasic rocks from this study and those reported in the literature to assess the relative contributions of metasedimentary versus metabasic rocks to deep N cycling.

2. Geological Background and samples

2.1 Geological Background

Tibet consists of the Kunlun-Qaidam terrane, the Songpan-Ganzi flysch complex, the North and South Qiangtang terrane(s) and the Lhasa terrane from north to south (Fig. 1). The epidote-blueschists and amphibolites studied here are from three locations in the central Qiangtang metamorphic belt – Gangma, Rongma and Shuang Hu from the west to the east. These metabasites are part of a tectonized mélange with dominantly siliciclastic metasedimentary matrix with blocks and tectonized slivers that include Paleozoic-Triassic strata, sandstone, marble, ophiolitic rocks and amphibole-, blueschist- and eclogite-facies metabasites and schists (Kapp and Decelles, 2019 and references therein). The high-pressure metamorphism in the mélange took place between 244 and 230 Ma during either the southward subduction of the Paleo-Tethys ocean beneath the Qiangtang terrane (Kapp et al., 2003; Pullen et al., 2008) or dominantly northward subduction of an ocean basin between the South and North Qiangtang terranes (Li et al., 1995; Zhang et al., 2006; Wu et al., 2016). Recognition of metamorphosed upper Paleozoic Qiangtang continental margin strata and fragments of continental basement in the CQMB raise the possibilities that oceanic subduction tectonically eroded the upper continental plate (Kapp et al., 2003; Zhang et al., 2017)

and/or was transitioning into continental margin subduction (Zhang et al., 2006; Xu et al., 2021). Metabasites in the CQMB consist of both blocks and strongly-sheared matrix within a sediment-rich block-in-matrix mélange (e.g., Kapp et al., 2003).

It has been recognized that at least a portion of the metasedimentary lithologies in the mélange have similar lithologies and detrital zircon signatures to unmetamorphosed Gondwana-affinity upper Paleozoic continental margin strata in the upper plate (e.g. Kapp et al., 2003; Tang and Zhang, 2014). These observations have been used to suggest that Qiangtang mélange includes subducted Gondwana-affinity continental margin strata and thus records the transition from oceanic subduction to continental subduction (Zhang et al., 2014; Liu et al., 2017; Xu et al., 2021). Upper Paleozoic strata include mafic lithologies in the form of intracontinental rift-related mafic sills and mafic volcanic and volcaniclastic sequences that were interlayered with upper Paleozoic continental margin clastic and carbonate strata of the Qiangtang terrane (Kapp et al., 2003; Pullen et al., 2008). These upper plate mafic lithologies may serve as potential protoliths to the metabasites analyzed in this study. However, geochemical studies on Qiangtang metabasites have been used to argue that their protoliths are E-MORB and OIB-type oceanic crust (Zhai et al., 2011; Zhang et al., 2017; Dan et al., 2018; Tian et al., 2023). In the absence of demonstrable data supporting a continental margin affinity for the metabasites, we follow previous interpretations of geochemical indicators that they represent fragments of metamorphosed oceanic crust. Everywhere studied in detail, high-pressure rocks of the CQMB were exhumed structurally beneath lowergrade upper Paleozoic - Triassic Qiangtang continental margin strata in the footwalls of domal low-angle normal faults (between ~ 225 and 204 Ma; Kapp et al., 2000, 2003; Liang et al., 2017). This structural setting requires the CQMB rocks to have underplated the Qiangtang continental margin, presumably during a phase of relatively shallowdepth flat-slab subduction (Kapp et al., 2003).

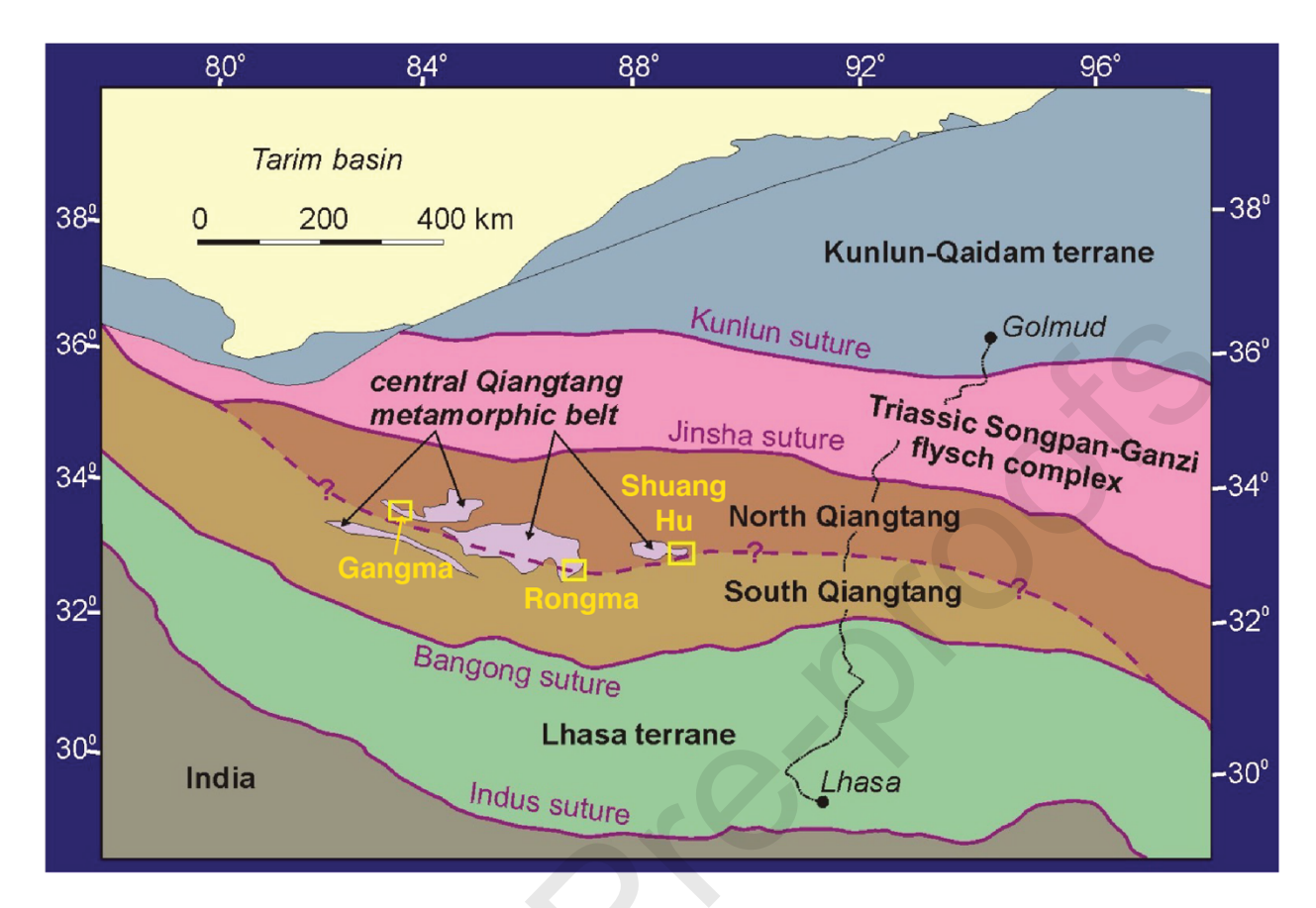


Figure 1. Geological map of Tibet (modified from Kapp et al., 2003). Yellow boxes show areas from which samples have been studied here.

2.2 Samples

We analyzed four amphibolite blocks from Shuang Hu and two strongly-sheared matrix epidote blueschists from each of the three localities (Rongma, Shuang Hu and Gangma). Details about the sample locations and petrography were previously reported by Kapp et al., (2003). The epidote blueschists from Shuang Hu and Gangma show signs of retrogression, including green amphibole (actinolite) rims or overgrowths on blue amphibole (glaucophane-rich) and fine-grained crystallization of matrix chlorite. The amphibolites from Shuang Hu and epidote blueschists from Rongma do not show any signs of retrogression. We selected a few potentially retrogressed samples along with unretrogressed ones to assess whether the process of retrogression may impart any systematic geochemical signature in terms of nitrogen abundance and isotopes.

Petrographic images of the samples from this study are included in Supplementary Information. The epidote blueschists contain plagioclase, chlorite, quartz, epidote, blue amphibole (glaucophane), clinopyroxene, sphene, with or without muscovite, calcite, rutile, ilmenite and apatite. Biotite (a potential key N hosting mineral) is noticeably absent from the epidote blueschists. Garnet is absent from all but one (Sample 6-30-99-2D) epidote blueschist. As discussed previously, the effect of retrogression is visible by

the rimming of glaucophane by actinolite. The amphibolites contain plagioclase, quartz, epidote, hornblende, biotite, sphene, rutile, with or without chlorite, calcite, clinopyroxene, garnet, Fe-Ti oxide, apatite and pyrite. Muscovite (another potentially key N hosting mineral) is noticeably absent from all the amphibolites.

Kapp et al., (2003) performed thermobarometry on these rocks. The study determined a peak condition of 11 kbar, 660 °C for the amphibolites and 14 kbar, 500 °C for the epidote blueschists.

3. Analytical methods

3.1 Major and trace elements

Bulk chemical analysis on all samples was done by Wavelength Dispersive X-Ray Fluorescence (WDXRF) at Hamilton Analytical Lab. WDXRF determinations were made with low-dilution (1:2 sample to flux ratio with Li-tetraborate only) doubly fused glass beads made using an adaptation of the preparation method described by Johnson et al. (1999); the usual mass of each sample is 3.5 grams for a 29 mm bead, less for a 15 mm bead. The chief difference is in the use of diamond polishing, rather than SiC grit, to create the analytical surface. First fused beads are re-ground to powder in a tungsten carbide ringmill for 30 seconds and fused again; both fusions occur under static conditions in a 1000 °C muffle furnace. The flat surface of the doubly fused bead was ground to a 15 μ finish on diamond lapping plates and sonicated in ethanol before set for analysis in the WDXRF spectrometer.

For WDXRF determinations, single backgrounds for each element were measured, and background was subtracted with formulas derived from pure element spike experiments. Equal time was spent counting peak and background positions for all elements. Total analytical time per bead was approximately 130 minutes. All intensities were collected at 45 kV and 45 mA. Spectral interferences were corrected with net intensity ratio factors or formulas derived from experiments with pure element spikes doped into either SiO_2 or Al_2O_3 matrices. LOI-eliminated influence coefficients were used for matrix correction. Calibration was done using the intensities gathered from 77 CRMs and RMs, chiefly those issued by the USGS and GSJ, but also including RMs from the CRPG, GIT-IWG, NIST, BAS, Mintek, and other sources. The revised USGS, GSJ, and CRPG CRM values provided in Jochum et al., (2016) were used and weighted more heavily than the values from other CRMs. Repeated analysis of internal standards and samples gave an analytical error (2 σ) of \leq 6% of the absolute value for major and minor elements and 1-215% for trace elements (the highest error is for Cs).

Further details of the calibration procedure and validation of the WDXRF method can be accessed at https://www.hamilton.edu/academics/analytical-lab.

3.2 Nitrogen abundance and isotopes

Nitrogen concentrations and isotope compositions were analyzed at University of Alberta following the technique by L.Li et al. (2021b). Sample powders were loaded together with CuO reagent and quartz wool in a one end-sealed quartz tube, which was put on a metal manifold to pump overnight. The sample tube was then sealed under high vacuum and combusted at 900 °C for 8 hours followed by 600 °C for 2 hours for a complete extraction of N in the blueschist samples and turning it into N₂ (L. Li et al., 2021b). The sample tube was subsequently cracked in a tube cracker in the metal manifold under high vacuum. The N₂ product was cryogenically purified, quantified by a capacitance manometer, and sent by a high-purity helium stream to a Thermo Finnegan MAT 253 isotope ratio mass spectrometer for isotopic analysis. The analyses of samples were calibrated by two OAS reference materials - high organic content sediment (N concentration of 0.52 wt.%, δ^{15} N = +4.32‰) and low organic content sediment (N concentration of 0.122 wt.%, δ^{15} N = +5.78‰). Repeated analysis of the samples gave an analytical error (2 σ) of <5% of the absolute value for N concentrations and <0.2‰ for δ^{15} N values.

4. Results

4.1 Trace elements and nitrogen geochemistry

We report the bulk major and trace element chemistries along with N abundances and isotopic ratios of the samples in Table 1.

We obtained 14-147 ppm N and δ^{15} N values from +1.8‰ to +10.0 ‰ in the metabasic rocks from this study (Fig. 2a). The Shuang Hu amphibolites show a range of N abundance from 21 – 147 ppm and δ^{15} N values from +3.1‰ to +9.1‰. The Rongma epidote blueschists show a range of N abundance from 14 – 43 ppm and δ^{15} N values from +1.8‰ to +8.0‰. The two retrogressed epidote blueschists from Shuang Hu show N abundances of 24 and104 ppm, and δ^{15} N values of +5.7‰ and +7.2‰. The two retrogressed epidote blueschists from Gangma show N abundances of 44 and 93 ppm and δ^{15} N values of +3.7‰ and +10.0‰. We observe positive correlations between N and Ba (Fig. 2b), N and Rb (Fig. 2c), N and K₂O (Fig. 2d), and N and Th abundances (Fig. 2e), and no correlations were observed between N abundances and δ^{15} N (Fig. 2a).

Table 1. Compositions of metabasic rocks from this study

SampleID	5-30-98- 11F	Repe- at	5-30-98- 11E	Repe- at	6-13-97- 3A	97-6-16- 4A	97-6-16- 4B	6-13-97- 3B	97-6-14- 1PK	5-30-99- 4	5-28-99- 4B	6-13- 97-2	6-30-99- 2D	Repe- at
Rock type	E-BS-R		E-BS-R		Α	Α	Α	Α	A-R	E-BS	E-BS	E-BS-R	E-BS	
	Matrix, foliated		Matrix, foliated		Block, foliated	Block, foliated	Block, foliated	Block, weakly foliated	Matrix, foliated	Matrix, undeform ed	Matrix, weakly foliated	Matrix, undefor med	Matrix, foliated	
Location	Gangma		Gangma		Shuang hu	Shuang hu	Shuang hu	Shuang hu	Shuang hu	Rongma	Rongma	Shuang hu	Rongma	
N (ppm)	44.0	44.3	93.2	98.3	91.1	21.0	27.5	147.3	23.8	42.7	41.4	103.7	14.4	14.1
δ ¹⁵ N ‰	10.0	9.7	3.7	3.7	5.6	6.6	9.1	3.1	5.7	3.7	1.8	7.2	8.0	8
SiO ₂ (wt.%)	45.8		46.5		47.6	47.2	49.2	40.5	42.9	45.4	42.6	45.8	44.7	
TiO ₂	4.2		3.4		1.3	2.3	0.2	6.3	4.4	4.5	3.5	4.4	2.9	
Al ₂ O ₃	10.3		10.6		12.0	13.2	16.4	10.6	6.2	15.6	8.6	10.3	8.1	
FeO	7.9		7.0		7.8	7.3	2.9	9.1	8.1	8.1	7.8	8.4	7.9	
Fe ₂ O ₃	4.9		4.2		4.0	5.1	1.3	4.8	5.0	4.2	5.1	4.7	4.7	

MnO	0.2	0.1	0.2	0.1	0.1	0.2	0.2	0.2	0.2	0.2	0.2
MgO	8.8	7.2	12.4	6.9	10.6	6.3	15.0	4.0	13.2	9.0	9.0
CaO	9.9	10.9	7.0	9.0	14.8	11.4	10.5	9.2	11.0	9.5	8.3
Na₂O	2.5	2.6	1.0	3.4	1.6	1.9	0.6	3.2	1.7	2.5	4.9
K ₂ O	2.0	2.7	0.7	0.7	0.4	2.9	0.8	1.3	1.0	1.1	b.d.l
P ₂ O ₅	0.5	0.4	0.1	0.8	b.d.l	1.8	0.5	0.3	0.5	0.6	b.d.l
LOI	2.9	3.7	4.7	2.3	1.5	2.4	4.8	2.6	4.1	2.6	6.4
F (ppm)	831	630	738	720	239	1890	1289	556	1147	931	644
CI	91	21	193	386	72	47	29	65	88	23	20
Br	2	2	2	2	1	2	2	2	2	2	2
As	4	3	29	4	b.d.l	b.d.l	b.d.l	b.d.l	b.d.l	7	b.d.l
S	241	96	260	4831	101	284	111	114	115	624	307
Ni	151	138	262	20	132	22	664	57	538	244	52
Cr	288	282	943	63	1253	b.d.l	1252	b.d.l	1021	421	53

V	346	336	271	96	158	540	311	727	316	364	285	
Sc	33	25	29	37	44	30	29	34	29	27	34	
Cu	55	103	103	6	63	114	113	159	125	158	34	
Zn	79	53	54	71	b.d.l	111	82	75	69	91	108	
Ga	22	21	15	22	9	28	16	23	17	23	12	
Ва	344	645	205	110	18	1204	221	257	471	310	9	
Rb	43	56	22	14	8	81	25	32	23	34	1	
Cs	b.d.l	1	b.d.l	3	b.d.l	b.d.l	2	12	b.d.l	1	b.d.l	
Sr	358	399	222	122	150	1381	167	534	309	218	89	
Y	31	26	18	72	9	54	25	25	27	32	16	
Zr	327	247	89	358	14	816	383	156	270	384	86	
Hf	9	5	2	9	0	21	9	4	8	10	2	
Nb	48	37	6	34	0	135	71	22	47	67	5	
Та	5	5	b.d.l	7	2	12	6	1	2	7	4	

Мо	3	2	1	2	2	5	2	2	2	2	1	
La	46	30	13	37	b.d.l	149	65	18	43	64	31	
Се	113	70	26	98	9	346	151	45	94	141	57	
Nd	57	39	15	52	4	172	73	24	45	67	23	
Th	8	5	4	11	1	22	10	4	4	6	1	
U	3	4	1	3	b.d.l	7	5	4	4	4	1	
Pb	4	4	5	6	2	12	4	b.d.l	1	9	2	
ТІ	b.d.l	2	3	1	0	b.d.l	b.d.l	1	b.d.l	3	2	

'repeat' - repeat analyses of N concentration and isotope of samples 5-30-98-11F, 5-30-98-11E, 6-30-99-2D; SiO_2 to LOI reported in wt.%; F to TI reported in ppm; 'E-BS' - Epidote blueschist; 'R' - retrogressed; 'A' - Amphibolite; b.d.l. below detection limit

5. Discussion

5.1 Nitrogen addition by metamorphic fluids followed by devolatilization

We obtained 14-147 ppm N and δ^{15} N from +1.8% to +10.0 % in the metabasic rocks from this study (Fig. 2a). The measured N abundance of 147 ppm in the mafic amphibolite from Shuang Hu is the highest reported for metabasic rocks thus far (Halama et al., 2010; Busigny et al., 2011; K. Li et al., 2021).

We observe a lack of correlation between N abundances and metamorphic temperatures in the samples from this study, in the sense, N abundances are not systematically higher or lower for higher (amphibolites) or lower (epidote blueschists) metamorphic temperatures. Also, the amphibolites from Shuang Hu show a range of N concentrations from 21 – 147 ppm which is indicative of fluid-rock interactions imparting N heterogeneously at a local scale, similar to that observed by K. Li et al. (2021). Retrogressed samples do not show systematically higher or lower N abundances, hence the effect of retrogression on N behavior during exhumation is not clear from this study.

The positive correlations between N and K_2O as well as N and Rb (Fig. 2d and c) confirm that N is mostly hosted as NH_4^+ in the silicate minerals by substituting for K^+ or Rb^+ (such as biotites and amphiboles), given they have similar ionic radii (NH_4^+ = 1.54 Å from Sidey, 2016; K^+ = 1.65 Å and Rb^+ = 1.75 Å from Shannon, 1976) and the same ionic charge of +1 (e.g. Busigny and Bebout, 2013). Biotites and amphiboles are likely the major hosts of N in the amphibolites. In the epidote blueschists, amphiboles and chlorite are perhaps the major hosts of N. Although chlorites are not alkali bearing minerals, Harris et al. (2022) demonstrated that chlorite may host several tens of ppm of N as NH_4^+ in its interlayered vacancies. The positive correlation between N and Ba as well as N and Th abundances (Fig. 2b and e) indicate that fluids were the carrier of N into or out of the rocks. These correlations were also observed in the metabasic rocks studied by Busigny et al. (2011) and K. Li et al. (2021).

The N concentrations in the amphibolites and epidote blueschists are overall higher than those reported for altered oceanic crust where the median abundance is 6.0 ± 4.7 ppm (Busigny et al., 2005, 2019; Li et al., 2007; Bebout et al., 2018; Li and Li, 2022, 2023b, a) which likely implies that most of the N is neither magmatic nor was introduced during hydrothermal alteration, but was rather introduced by metamorphic fluids in the subduction channel. To further confirm that most of the N in the metabasic rocks was acquired by metamorphic fluids, we also examined their trace element systematics to understand whether the trace element characteristics align with the effects from

metamorphic fluids. As compared to hydrothermal alteration on the seafloor, metamorphism results in lowering of K₂O, thus in a plot of K₂O/Th versus Ba/Th, metamorphic fluid alteration results in a lower slope than seafloor hydrothermal alteration (Bebout, 2007). Also, Th is added to the system by metamorphic fluids resulting in Th enrichment and a shallower slope in Th/U versus Th as compared to seafloor hydrothermal alteration (Bebout, 2007). Both K₂O and Rb are enriched during seafloor hydrothermal alteration but Ba is not as enriched due to its lower mobility in hydrothermal fluids compared to K and Rb, however, Ba may be as mobile as Rb in metamorphic fluids (e.g. Seyfried et al., 1998). Thus in a plot of Ba/Rb versus K₂O, hydrothermal fluids show a decreasing slope while metamorphic fluid alteration shows a flat trend (van der Straaten et al., 2012). In plots of Ba/Rb versus K₂O, K₂O/Th versus Ba/Th, and Th/U versus Th, the metabasic samples from this study lie along the trends for metamorphic fluid alteration (Fig. 3) indicating that the trace element signatures in the metabasic rocks were inherited during metamorphism in the subduction channel rather than on the seafloor. Thus, it is more likely that the N signatures (both in terms of concentration and isotopic ratio) of these metabasic rocks could have been imprinted in the subduction channel during metamorphism rather than during hydrothermal alteration prior to subduction. This observation is similar to that of the blueschist rocks from the Heilongjiang Complex in northeast China (K. Li et al., 2021).

The N abundances of the metabasic rocks from this study are in between that of altered oceanic crust and the median N abundances of metasediments (Fig. 2). Also the δ^{15} N being positive for the rocks indicate that the fluids that carried N were likely sourced from metasediments. The metasediments could either be tectonically eroded from the upper plate in the subduction channel (e.g. Zhang et al., 2017), or they could be sliced segments of overlying continental basement in the subduction channel mélange (e.g. Kapp et al., 2003) in case of Cordilleran-type oceanic subduction, or they may consist of surrounding continental lithologies in case of continental subduction (Kapp et al., 2003; Xu et al., 2021).

The $\delta^{15}N$ of the metabasic rocks from this study are overall higher than the median of metasediments and altered oceanic crust as reported in the literature, and the enrichment in ^{15}N over what may have been acquired by metasedimentary fluids needs to be explained. The fact that a negative correlation exists between N abundance and $\delta^{15}N$ for the epidote blueschists from Rongma and amphibolites from Shuang Hu may be indicative that after N was acquired from metasedimentary fluids, some of the metabasic rocks underwent devolatilization which resulted in the simultaneous loss of N and enrichment of ^{15}N in the residue. To test this hypothesis, we modeled batch and Rayleigh devolatilization of the amphibolites from Shuang Hu and epidote blueschists from Rongma (Fig. S1), using an approach similar to that by Halama et al. (2010). We find that the progressive ^{15}N enrichment and the simultaneous loss of N in the epidote blueschists of Rongma and amphibolites from Shuang Hu may be explained either by Rayleigh or batch devolatilization during metamorphism.

To sum it up, it appears that a two-step process led to N acquisition in the metabasic rocks from this study. In the first step, the metabasic rocks acquired their N from metasediment-derived fluids during metamorphism in the subduction channel. In the second step, some of the metabasic rocks underwent N loss and concomitant enrichment in ¹⁵N due to devolatilization within the subduction channel.

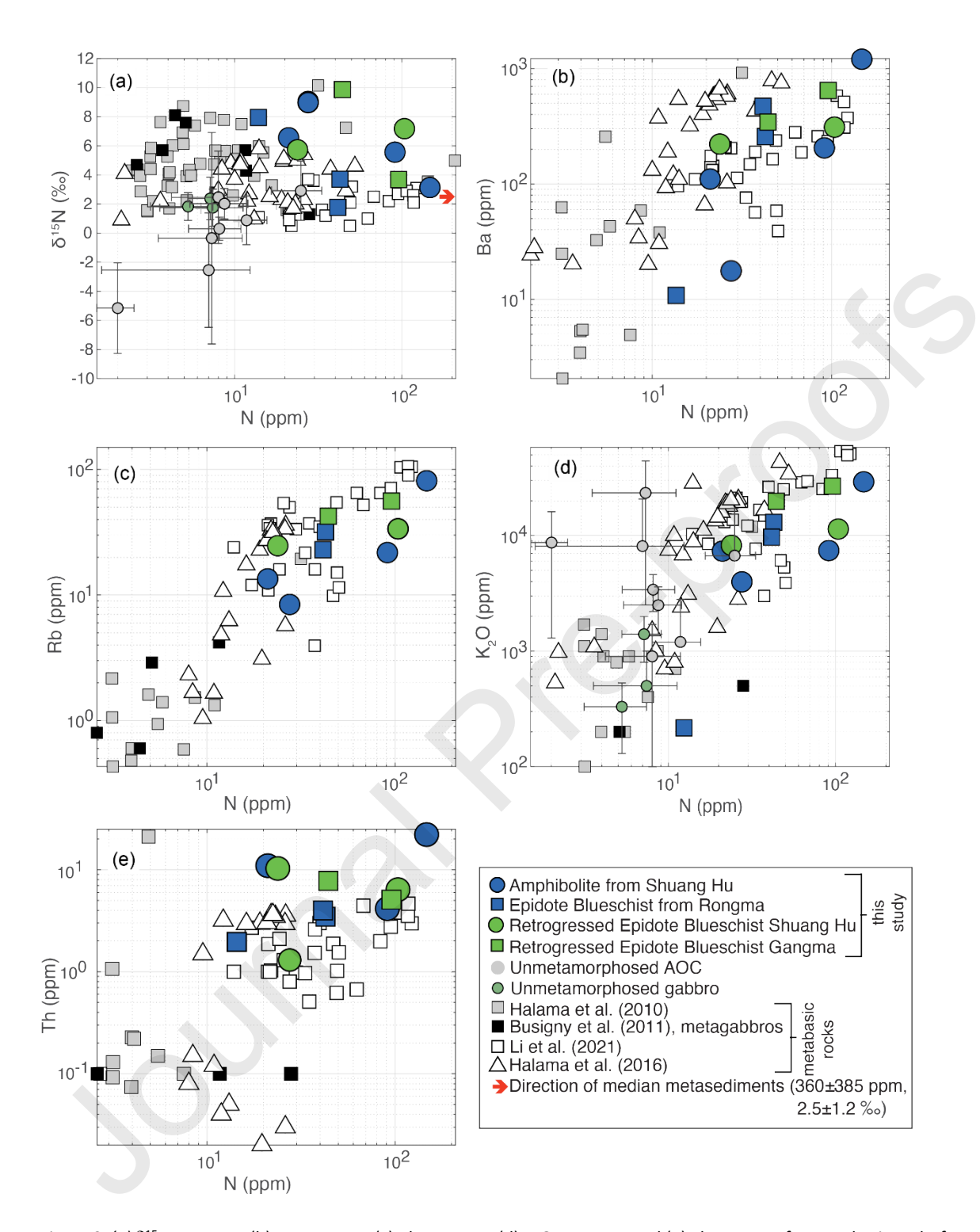


Figure 2. (a) δ^{15} N versus N, (b) Ba versus N, (c) Rb versus N, (d) K₂O versus N, and (e) Th versus N for metabasic rocks from this study along with unmetamorphosed altered oceanic crust and metabasic rocks reported by previous studies. Major and trace element concentrations for subducted-metabasic rocks are from Tianshan Belt (Beinlich et al., 2010; van der Straaten et al., 2012), Raspas Complex and Cabo Ortegal (Halama et al., 2010), Zambezi Belt (John et al., 2004), Piemonte-Ligurian domain in western Alps (Busigny et al., 2011), Heilongjiang complex (K. Li et al., 2021). δ^{15} N (‰) and N concentrations (ppm) in metabasic rocks are from Tianshan Belt (Halama et al., 2017), Piemonte-Ligurian domain in western Alps (Busigny et al., 2011), Heilongjiang complex (K. Li et al., 2021), Raspas Complex, Lago di Cignana, Zambezi Belt, and Cabo Ortegal (Halama et al., 2010). Fig. 2(a) does not show additional two metabasic rocks from Heilongjiang complex (K. Li et al., 2021) that have δ^{15} N (‰) of -10.9

and -10.1 with N concentrations of 46.9 and 39.7 ppm respectively. δ^{15} N (‰), N and K₂O concentrations (average and one-sigma standard deviation) of unmetamorphosed AOC are from Sites 801 and 1149 (Li et al., 2007), Hole 504B (Busigny et al., 2019), ODP Site 1256 (Bebout et al., 2018; Busigny et al., 2005; Li & Li, 2022), Holes 1224F, 543A, 417A, and 556 (Li & Li, 2023b). δ^{15} N (‰), N and K₂O concentrations (average and one-sigma standard deviation) of unmetamorphosed gabbros are from Holes 735B, 1309D and 1415P (Li and Li, 2023a). Median δ^{15} N (‰) and N abundance of metasediments are from references in the text.

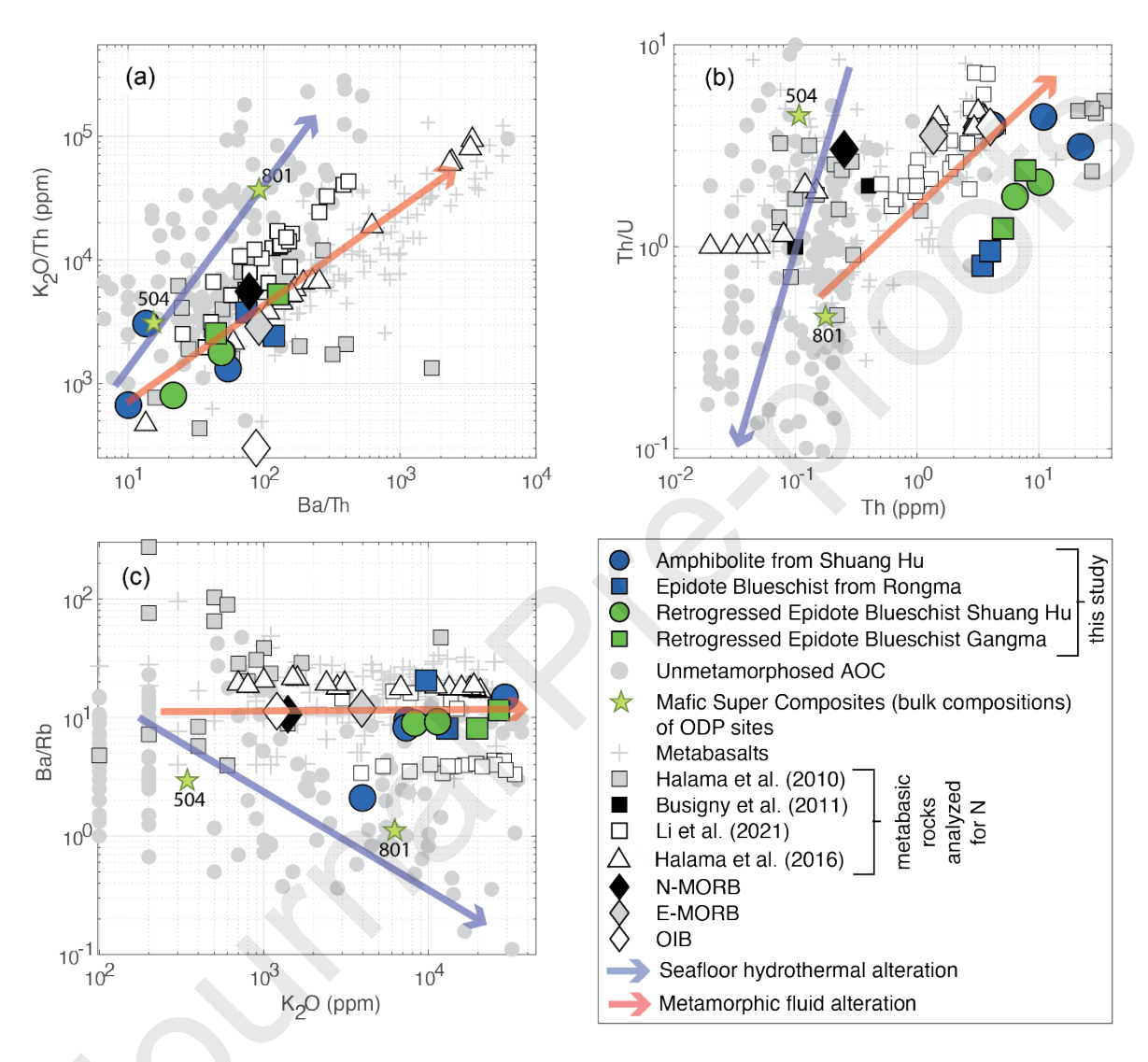


Figure 3. (a) K₂O/Th versus Ba/Th, (b) Th/U versus Th and (c) Ba/Rb versus K₂O for metabasic rocks from this study along with unmetamorphosed altered oceanic crust, metabasalts, and metabasalts that have been analyzed for nitrogen (Halama et al., 2010, 2017; Busigny et al., 2011; K. Li et al., 2021). The unmetamorphosed AOC data including both discrete and super composite data (seafloor hydrothermal alteration) are retrieved from ODP sites 801 and 1149 (Kelley et al., 2003), site 504 (Bach et al., 2003). The subduction-related metabasalts (metamorphic fluid alteration) are from the Zambezi Belt (John et al., 2004), Tianshan belt complex (Beinlich et al., 2010; van der Straaten et al., 2012), and Franciscan and Samana Complex (Sorensen et al., 1997). Also plotted are N-MORB (Gale et al., 2013), E-MORB (Gale et al., 2013) and OIB (Sun and McDonough, 1989) for reference. The seafloor hydrothermal and metamorphic fluid alteration trends are based on Bebout, (2007) and van der Straaten et al., (2012).

5.2 Significance of metabasic rocks in delivering nitrogen to forearc conditions

We modeled the delivery of N by metasedimentary and metabasic rocks in 55 presentday subduction zones (Hacker, 2008; Syracuse et al., 2010; van Keken et al., 2011) to assess the relative importance of metabasic rocks as compared to metasedimentary rocks as agents of nitrogen delivery to forearc conditions within the subduction channel. Even though N may be introduced in subduction zones by mafic rocks other than oceanic crust (such as those associated with volcanism in intracontinental margins), in this section we only consider N delivery by mafic oceanic crust during subduction. This is simply because the mass of oceanic crust being subducted globally is better constrained whereas the mass of mafic volcanics being subducted through continental subduction and also recycling rates in the mantle due to continental subduction are currently poorly quantified (e.g. Ducea, 2016). Towards the end of this section, we discuss that ignoring mafic rocks via continental subduction in our model would have no effect on our findings. We also do not consider delivery of N via serpentinized lithosphere in this study since the degree of serpentinization in the lithosphere is poorly constrained across subduction zones and we choose to avoid adding more uncertainty to our estimates.

We use subduction velocities, trench lengths, and sediment thicknesses for each subduction zone segment compiled by van Keken et al., (2011) to calculate the volume of sediment entering each trench and carried to fore-arc depths. The sediment thicknesses are originally from Clift and Vannucchi (2004) and Scholl and Von Huene (2007) and include the effects of sediment compaction and off-scraping in the accretionary prism. We assume mean densities of sediments entering each subduction zone from Plank and Langmuir (1998), except for Calabria where the mean sediment density is taken from Ocean Drilling Program Leg 107 drillsite 650 (Kastens et al., 1987), to calculate the masses of sediments entering the trenches and eventually carried to fore-arc depths. The oceanic crust is assumed to be 7 km thick, with 600 m of extrusives at the top, followed by 1.4 km of sheeted dikes and gabbro as the remainder (Jarrard, 2003) for each subduction zone segment. An additional scenario is considered where 25% mass loss (based on the lower estimate of Ague, 2011) due to dehydration of sediments during forearc processing, mélange formation and metamorphism (including H₂O, N, Si, Al etc.) is accounted for along with the internal redistribution of the mass (i.e. uptake of the sediment-derived mass by mafic lithologies).

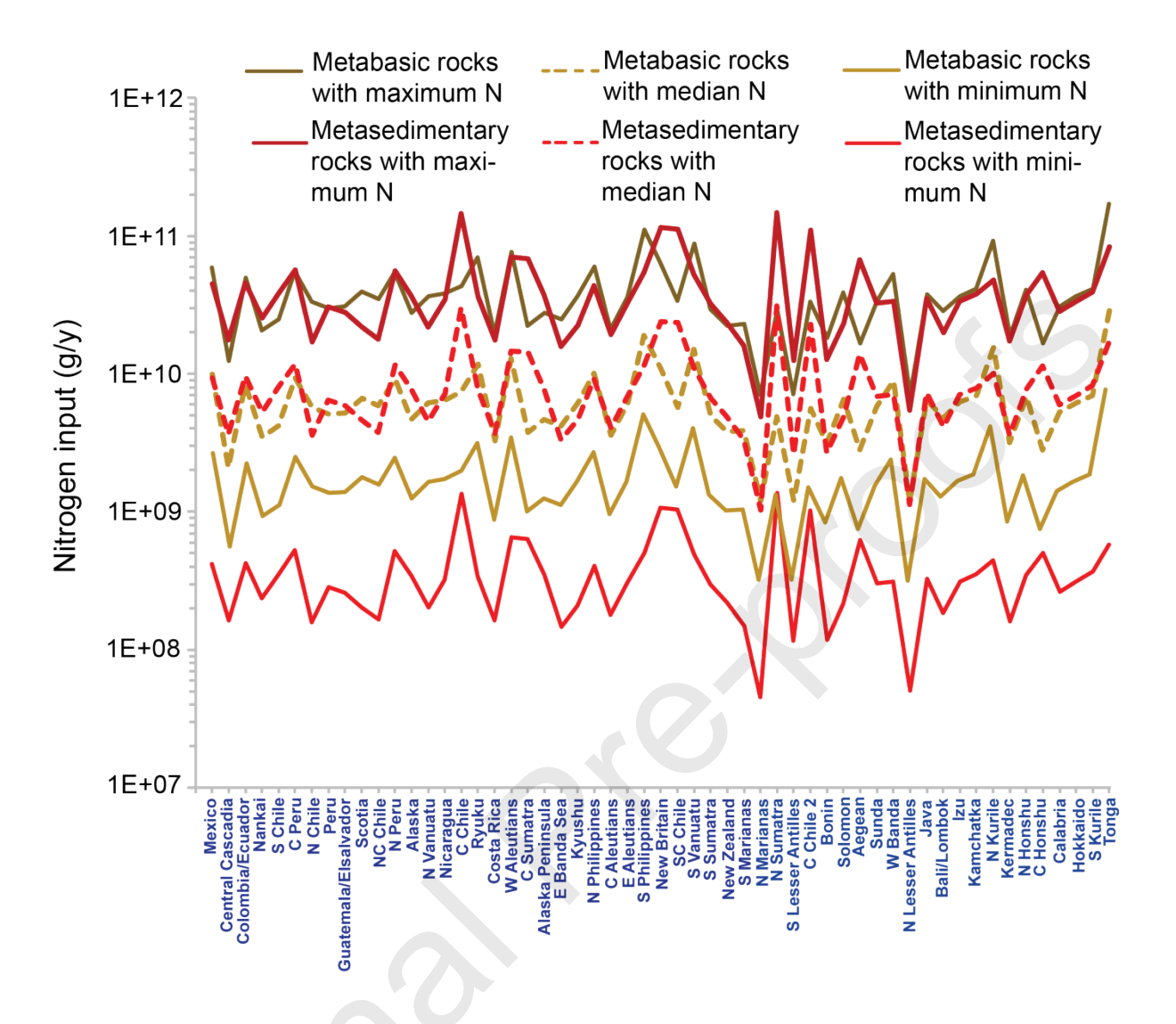


Figure 4. Nitrogen delivery fluxes at fore-arc depths (in grams/year) across 55 subduction zones today where the subduction zones are arranged from left to right according to decreasing slab-top temperatures at 100 km depth (based on model D80 of Syracuse et al., 2010). The maximum, median and minimum N concentrations in metasedimentary rocks are 1721, 360 and 16 ppm respectively (see text for references). For metabasic rocks, the sheeted dikes and basaltic lavas have maximum, median and minimum N concentrations of 147 (this study), 12 and 2 ppm respectively (see text for references). The gabbros have 5.9 ppm N concentrations (Busigny et al., 2011) for the maximum and median estimates and 2 ppm for the minimum estimate.

We consider the maximum (147 ppm for meta-basalt and -sheeted dikes from this study; 1721 ppm for metasediments from Busigny et al., 2003), minimum (2 ppm for meta-basalt and -sheeted dikes from Halama et al., 2017; 16 ppm for metasedimentary rocks from Bebout, 1997) and median N concentrations (360 ppm for metasedimentary and 12 ppm for meta-basalt and -sheeted dikes) in the subducted lithologies to estimate the fluxes of N in subduction zones (Table 2, Table S1). Due to their proximity to sediments, the gain of N from sedimentary components is more likely in metamorphosed basalts and sheeted dikes than metagabbro. Thus, it is reasonable to assume that the N concentrations in metagabbros would be at least equal to or lower than the N concentrations in meta-basalts and -sheeted dikes. Accordingly, we have considered 5.9 ppm (the median concentration from Busigny et al., 2011) as the N

concentration in metagabbro for the maximum and median deliveries above, and 2 ppm (the same as the lowest N abundance in metasediments) for the minimum delivery via metagabbros. The reason why we consider the range in concentrations as opposed to only the median is explained as follows. The N concentrations reported in the literature (including this study) for metasediments and metabasic rocks display highly positively skewed distributions: 43% of the data from metasedimentary rocks have concentrations within 266 ppm while 70% of the data from metabasic rocks lie within 22 ppm. Whether the skewed distributions represent the actual delivery across subduction zones globally or they are heavily biased by sampling is yet to be determined, especially since this study is the second to report N contents in metabasic rocks that exceed 100 ppm (the first one being Li et al., 2022). Therefore, this highlights the importance of studying N behavior in metamorphic rocks in more locations globally. A fallout of the highly skewed distribution is that standard deviations are largely overestimated, hence, we use the range in the data to estimate fluxes. We do however acknowledge that until the validity of the skewness in distribution is established by future studies, it is more logical to use the median concentrations to better understand the overall deep cycling of N in subduction zones. The range of concentrations encompass a realm of possibilities including (a) some N could be lost by sediments during metamorphism and taken up by metabasic rocks, as supported by Halama et al., (2021), K. Li et al., (2021) and this study, so a closed system scenario where no net loss of N takes place from the system; (b) N may be lost from the metasediments and metabasic rocks in the mélange by dehydration and fore-arc depth partial melting (for very hydrous sediments in hot subduction zones), so an open system scenario where net N loss takes place from the system. Therefore, the calculated N fluxes via metasedimentary rocks represent the rate of N delivery at forearc depths after the loss to metabasic rocks or from the system itself (where the system consists of metasediments and metabasic rocks). The calculated N fluxes for metabasic rocks represent the amount of N carried to forearc depths either after gaining from metasediments, or some N inherited during alteration on the seafloor (e.g. Halama et al., 2010a), or likely N lost from the system during metamorphic devolatilization (e.g. Halama et al., 2010a). The calculated fluxes are reported in Table 2.

We find that for maximum and minimum N concentrations, the N delivery at forearc depths through metasediments are 2.3×10^{12} g/y and 2.1×10^{10} g/y respectively, and through metabasic rocks are 2.2×10^{12} g/y and 9.8×10^{10} g/y respectively. The N delivery fluxes via median concentrations of N are 4.9×10^{11} g/y and 3.7×10^{11} g/y for metasediments and metabasic rocks respectively. Accounting for the redistribution of masses between metasediments and metabasic rocks during metamorphism, the N delivery fluxes via median concentrations of N are 3.6×10^{11} g/y and 3.7×10^{11} g/y for metasediments and metabasic rocks respectively. These fluxes imply that metabasic rocks, irrespective of their N contents, supply comparable amounts of N at forearc depths to metasediments even though metasedimentary rocks have at least an order of magnitude higher N concentration than metabasic rocks. Thus, metabasic rocks being a key player in N delivery to subduction zones further highlights the need to investigate N

behavior in metabasic rocks from more locations globally to obtain a better handle on deep N cycling.

The global median delivery flux of 3.7×10^{11} g/y for metabasic rocks from this study is comparable to 5.5×10^{11} g/y estimated by Busigny et al. (2011) (based on metabasic rocks from western Alps) and to input fluxes of $(2.9 - 4.2) \times 10^{11}$ g/y by unmetamorphosed mafic oceanic crust as reported by Li and Li (2023). The median concentrations of 12 ppm of N (this study) and 10.6 ppm (Busigny et al., 2011) in metabasic rocks used to estimate the above fluxes are comparable to the N concentrations of 6.6 - 10.6 ppm in unmetamorphosed mafic oceanic crust assumed by (Li and Li, 2023a).

The global N flux at forearc and subsequently to sub-arc conditions via metasediments and metabasic rocks (assuming the median N concentrations in metasediments and metabasic rocks) is 8.6×10^{11} g/y. This flux is comparable to 8.7×10^{11} g/y determined by Mallik et al., (2018) where they assumed the same subduction zone segments from van Keken et al., (2011) and comparable average N concentrations in sediments (424 ppm) and mafic crust (6 ppm in mafic extrusives and gabbros). In case at least some of the metabasic rocks from this study represent mafic sills and volcanics on continental margins (which cannot be entirely precluded based on their interlayering with upper Paleozoic continental margin clastic and carbonate strata of the Qiangtang terrane, Kapp et al., 2003; Tang and Zhang, 2014), adding mafic rocks due to continental subduction would increase the fluxes of N supply to forearc depths via metabasic rocks. Thus, the relative dominance of metabasic rocks in N delivery would still hold. Nevertheless, the large variation in N abundance in metabasic rocks from this study highlight the need to further investigate samples from more locations worldwide to better constrain the processes that govern N behavior during metamorphism and consequently obtain a more robust estimate of N delivery by them.

With the revised fluxes reported in this study, future studies need to re-evaluate the fluxes that are released from the subducting slab and their potential controlling factors (e.g., thermal structure) in individual subduction zones worldwide (Mallik et al., 2018; Förster et al., 2019; Jackson et al., 2021; Li and Li, 2022) to better estimate the N budgets during deep cycling. Constraining fluxes out of the slab requires detailed phase equilibria studies for the various mélange lithologies especially the modes and stabilities of key N hosting minerals, along with fluid-mineral and melt-mineral partition coefficients of N as a function of pressure, temperature and oxygen fugacity applicable for subducted slabs.

Table 2. Results of N flux calculations at fore-arc depths

Lithologic type	Maximum N concentratio n (ppm)	Median N concentratio n (ppm)	Minimum N concentratio n (ppm)	Flux from maximum N concentratio n (grams/year)	Flux from median N concentratio n (grams/year)	Flux from minimum N concentratio n (grams/year)	Flux from 25% mass redistributio n (grams/year
Metabasic	147, 5.9 *	12, 5.9 *	2, 2 *	2.2E+12	3.7E+11	9.8E+10	3.7E+11
Metasedimentar y	1721	360	16	2.3E+12	4.9E+11	2.1E+10	3.6E+11
Total (metabasic+ metasedimentar y)			8,	4.5E+12	8.6E+11	1.2E+11	7.4E+11

^{* -} x, y indicates x ppm in sheeted dikes and basalts, y ppm in gabbros

6. Concluding remarks

We investigate the N abundance, isotope compositions and trace element characteristics of amphibolites and epidote-blueschists from the Central Qiangtang Metamorphic Belt in Tibet which likely represent mafic rocks from the transition of oceanic to continental subduction. We find that the rocks acquired N from sedimentary or continental fluids during metamorphism within the subduction channel. It also appears that a two-step process led to N acquisition in the metabasic rocks. In the first step, the metabasic rocks acquired their N from metasediment-derived fluids during metamorphism in the subduction channel. In the second step, some of the metabasic rocks underwent N loss and concomitant enrichment in ¹⁵N due to devolatilization within the subduction channel. We then estimate the fluxes of N at fore-arc depths in modern-day subduction zones by metasedimentary and metabasic rocks. We find that metabasic rocks are comparable to metasedimentary rocks as carriers of N to

subduction zones which reinforces the need to investigate the behavior of N in metabasic rocks better for an improved understanding of global deep N cycling.

The fact that N in metabasic rocks from different locations globally show different scenarios of N behavior pre- and post-subduction highlight the importance of investigating a wider array of metabasic rocks from locations worldwide, and that N behavior inferred from a few locations may not be representative of deep N cycling at a global scale. This highlights the need for investigation of N characteristics in metabasic rocks from more locations to improve our understanding of deep N cycling due to subduction.

Acknowledgements

The authors acknowledge Zachary Michels for assistance with the SEM at Arizona Laserchron Center, Hamilton Analytical Laboratory for trace element analysis, Grindstone Laboratories for thin-section preparation, and Lisa Zieman for assistance with the shatterbox that was used for pulverizing samples. The authors acknowledge an anonymous reviewer, Kan Li and associate editor Ralf Halama for constructive reviews that substantially improved the manuscript. AM acknowledges National Science Foundation grant EAR 2138410, and her startup grant from the Office for Research, Innovation and Impact and Eminent Scholar Funds from the College of Science at the University of Arizona. AR acknowledges the David J. Lowell Scholarship from the University of Arizona. PK acknowledges National Science Foundation grant EAR 2048656. LL acknowledges an NSERC-Discovery Grant. EC acknowledges National Science Foundation grant EAR 2138484.

Data Availability

Data, including Supplementary Information, are available through University of Arizona Research Data Repository (ReDATA) at 10.25422/azu.data.23504415 .

References

- Ague J. J. (2011) Extreme channelization of fluid and the problem of element mobility during Barrovian metamorphism. *Am. Mineral.* **96**, 333–352.
- Bach W., Peucker-Ehrenbrink B., Hart S. R. and Blusztajn J. S. (2003) Geochemistry of hydrothermally altered oceanic crust: DSDP/ODP Hole 504B–Implications for

- seawater-crust exchange budgets and Sr-and Pb-isotopic evolution of the mantle. *Geochemistry, Geophys. Geosystems* **4,** 8904.
- Bebout G. E. (2007) Metamorphic chemical geodynamics of subduction zones. *Earth Planet. Sci. Lett.* **260**, 373–393.
- Bebout G. E. (1997) Nitrogen isotope tracers of high-temperature fluid-rock interactions: Case study of the Catalina Schist, California. *Earth Planet. Sci. Lett.* **151**, 77–90.
- Bebout G. E., Banerjee N. R., Izawa M. R. M., Kobayashi K., Lazzeri K., Ranieri L. A. and Nakamura E. (2018) Nitrogen Concentrations and Isotopic Compositions of Seafloor-Altered Terrestrial Basaltic Glass: Implications for Astrobiology. *Astrobiology* **18**, 330–342.
- Bebout G. E. and Barton M. D. (2002) Tectonic and metasomatic mixing in a high-T, subduction-zone mélange Insights into the geochemical evolution of the slabmantle interface. *Chem. Geol.* **187**, 79–106.
- Bebout G. E. and Fogel M. L. (1992) Nitrogen-isotope compositions of metasedimentary rocks in the Catalina Schist, California: Implications for metamorphic devolatilization history. *Geochim. Cosmochim. Acta* **56**, 2839–2849.
- Bebout G. E., Fogel M. L. and Cartigny P. (2013) Nitrogen: Highly Volatile yet Surprisingly Compatible. *Elements* **9**, 333–338.
- Beinlich A., Klemd R., John T. and Gao J. (2010) Trace-element mobilization during Cametasomatism along a major fluid conduit: Eclogitization of blueschist as a consequence of fluid-rock interaction. *Geochim. Cosmochim. Acta* **74**, 1892–1922.
- Busigny V. and Bebout G. E. (2013) Nitrogen in the silicate earth: Speciation and isotopic behavior during mineral-fluid interactions. *Elements* **9**, 353–358.
- Busigny V., Cartigny P., Laverne C., Teagle D., Bonifacie M. and Agrinier P. (2019) A re-assessment of the nitrogen geochemical behavior in upper oceanic crust from Hole 504B: Implications for subduction budget in Central America. *Earth Planet. Sci. Lett.* **525**, 115735.
- Busigny V., Cartigny P. and Philippot P. (2011) Nitrogen isotopes in ophiolitic metagabbros: A re-evaluation of modern nitrogen fluxes in subduction zones and implication for the early Earth atmosphere. *Geochim. Cosmochim. Acta* **75**, 7502–7521.
- Busigny V., Cartigny P., Philippot P., Ader M. and Javoy M. (2003) Massive recycling of nitrogen and other fluid-mobile elements (K, Rb, Cs, H) in a cold slab environment: evidence from HP to UHP oceanic metasediments of the Schistes Lustrés nappe (western Alps, Europe). *Earth Planet. Sci. Lett.* **215**, 27–42.
- Busigny V., Chen J., Philippot P., Borensztajn S. and Moynier F. (2018) Insight into

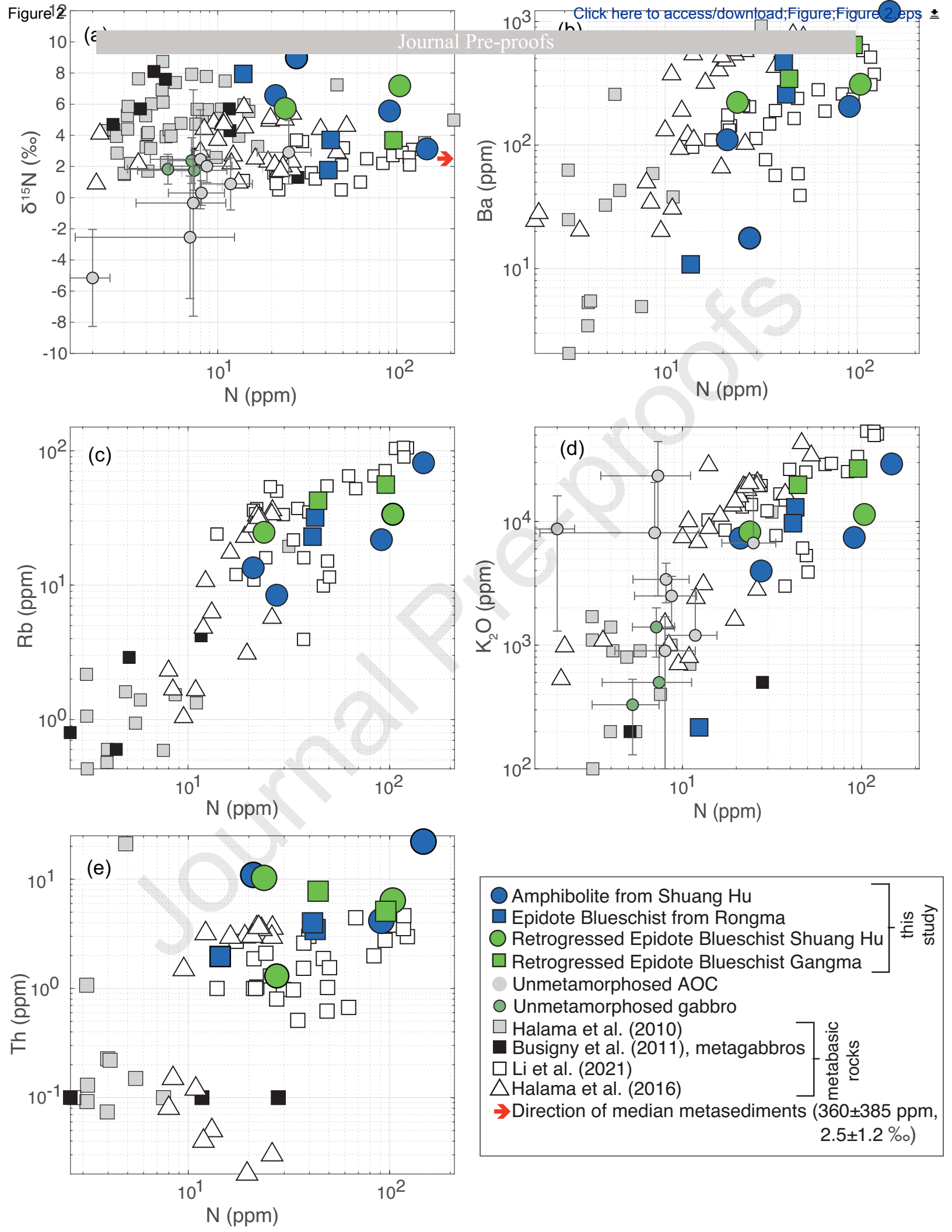
- hydrothermal and subduction processes from copper and nitrogen isotopes in oceanic metagabbros. *Earth Planet. Sci. Lett.* **498**, 54–64.
- Busigny V., Laverne C. and Bonifacie M. (2005) Nitrogen content and isotopic composition of oceanic crust at a superfast spreading ridge: A profile in altered basalts from ODP Site 1256, Leg 206. *Geochemistry, Geophys. Geosystems* **6**, Q12O01.
- Cannaò E., Tiepolo M., Bebout G. E. and Scambelluri M. (2020) Into the deep and beyond: Carbon and nitrogen subduction recycling in secondary peridotites. *Earth Planet. Sci. Lett.* **543**, 116328.
- Clift P. and Vannucchi P. (2004) Controls on tectonic accretion versus erosion in subduction zones: Implications for the origin and recycling of the continental crust. *Rev. Geophys.* **42**.
- Cooperdock E. H. G., Raia N. H., Barnes J. D., Stockli D. F. and Schwarzenbach E. M. (2018) Tectonic origin of serpentinites on Syros, Greece: Geochemical signatures of abyssal origin preserved in a HP/LT subduction complex. *Lithos* **296–299**, 352–364.
- Dan W., Wang Q., White W. M., Zhang X. Z., Tang G. J., Jiang Z. Q., Hao L. L. and Ou Q. (2018) Rapid formation of eclogites during a nearly closed ocean: Revisiting the Pianshishan eclogite in Qiangtang, central Tibetan Plateau. *Chem. Geol.* **477**, 112–122.
- Ducea M. N. (2016) RESEARCH FOCUS: Understanding continental subduction: A work in progress. *Geology* **44**, 239–240.
- Förster M. W., Foley S. F., Alard O. and Buhre S. (2019) Partitioning of nitrogen during melting and recycling in subduction zones and the evolution of atmospheric nitrogen. *Chem. Geol.* **525**, 334–342.
- Gale A., Dalton C. A., Langmuir C. H., Su Y. and Schilling J. G. (2013) The mean composition of ocean ridge basalts. *Geochemistry, Geophys. Geosystems* **14**, 489–518.
- Hacker B. R. (2008) H₂O subduction beyond arcs. *Geochemistry, Geophys. Geosystems* **9**, Q03001.
- Halama R., Bebout G. E. and Bea F. (2021) Nitrogen loss and isotopic fractionation during granulite-facies metamorphism in the lower crust (Ivrea Zone, NW Italy). *Chem. Geol.*, 120475.
- Halama R., Bebout G. E., John T. and Schenk V. (2010) Nitrogen recycling in subducted oceanic lithosphere: The record in high- and ultrahigh-pressure metabasaltic rocks. *Geochim. Cosmochim. Acta* **74**, 1636–1652.

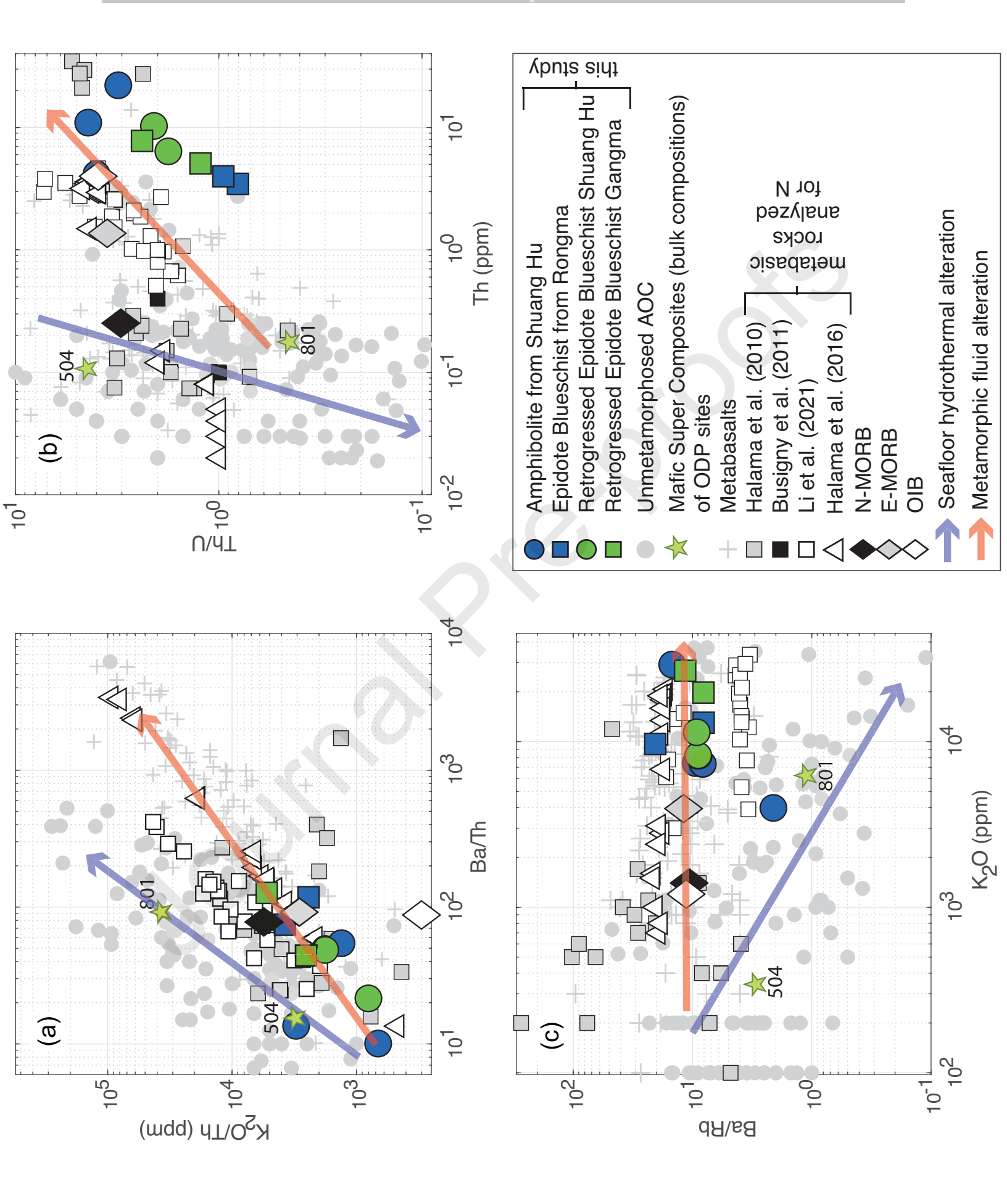
- Halama R., Bebout G. E., Marschall H. R. and John T. (2017) Fluid-induced breakdown of white mica controls nitrogen transfer during fluid—rock interaction in subduction zones. *Int. Geol. Rev.* **59**, 702–720.
- Harris B. J. R., de Hoog J. C. M. and Halama R. (2022) The behaviour of nitrogen during subduction of oceanic crust: Insights from in situ SIMS analyses of high-pressure rocks. *Geochim. Cosmochim. Acta* **321**, 16–34.
- Jackson C. R. M., Cottrell E. and Andrews B. (2021) Warm and oxidizing slabs limit ingassing efficiency of nitrogen to the mantle. *Earth Planet. Sci. Lett.* **553**, 116615.
- Jarrard R. D. (2003) Subduction fluxes of water, carbon dioxide, chlorine, and potassium. *Geochemistry*, *Geophys. Geosystems* **4**, 8905.
- Jochum K. P., Weis U., Schwager B., Stoll B., Wilson S. A., Haug G. H., Andreae M. O. and Enzweiler J. (2016) Reference Values Following ISO Guidelines for Frequently Reguested Rock Reference Materials. *Geostand. Geoanalytical Res.* **40**, 333–350.
- John T., Scherer E. E., Haase K. and Schenk V. (2004) Trace element fractionation during fluid-induced eclogitization in a subducting slab: Trace element and Lu-Hf-Sm-Nd isotope systematics. *Earth Planet. Sci. Lett.* **227**, 441–456.
- Johnson D. M., Hooper P. R. and Conrey R. M. (1999) XRF analysis of rocks and minerals for major and trace elements on a single low dilution Li-tetraborate fused bead. *Adv. X-ray Anal.* **41**, 843–867.
- Kapp P. and Decelles P. G. (2019) Mesozoic–Cenozoic geological evolution of the Himalayan-Tibetan orogen and working tectonic hypotheses. *Am. J. Sci.* **319**, 159–254.
- Kapp P., Yin A., Manning C. E., Harrison T. M., Taylor M. H. and Ding L. (2003) Tectonic evolution of the early Mesozoic blueschist-bearing Qiangtang metamorphic belt, central Tibet. *Tectonics* **22**, 1043.
- Kapp P., Yin A., Manning C. E., Murphy M., Harrison T. M., Spurlin M., Lin D., Xi-Guang D. and Cun-Ming W. (2000) Bluechist-bearing metamorphic core complexes in the Qiangtang block reveal deep crustal structure of northern Tibet. *Geology* **28**, 19–22.
- Kastens K. A., Mascle J., Auroux C. and (1987) Site 650: Marsili Basin. In *Proceedings of the Ocean Drilling Program, 107 Initial Reports* Ocean Drilling Program.
- van Keken P. E., Hacker B. R., Syracuse E. M. and Abers G. A. (2011) Subduction factory: 4. Depth-dependent flux of H2O from subducting slabs worldwide. *J. Geophys. Res. Solid Earth* **116,** B01401.
- Kelley K. A., Plank T., Ludden J. and Staudigel H. (2003) Composition of altered

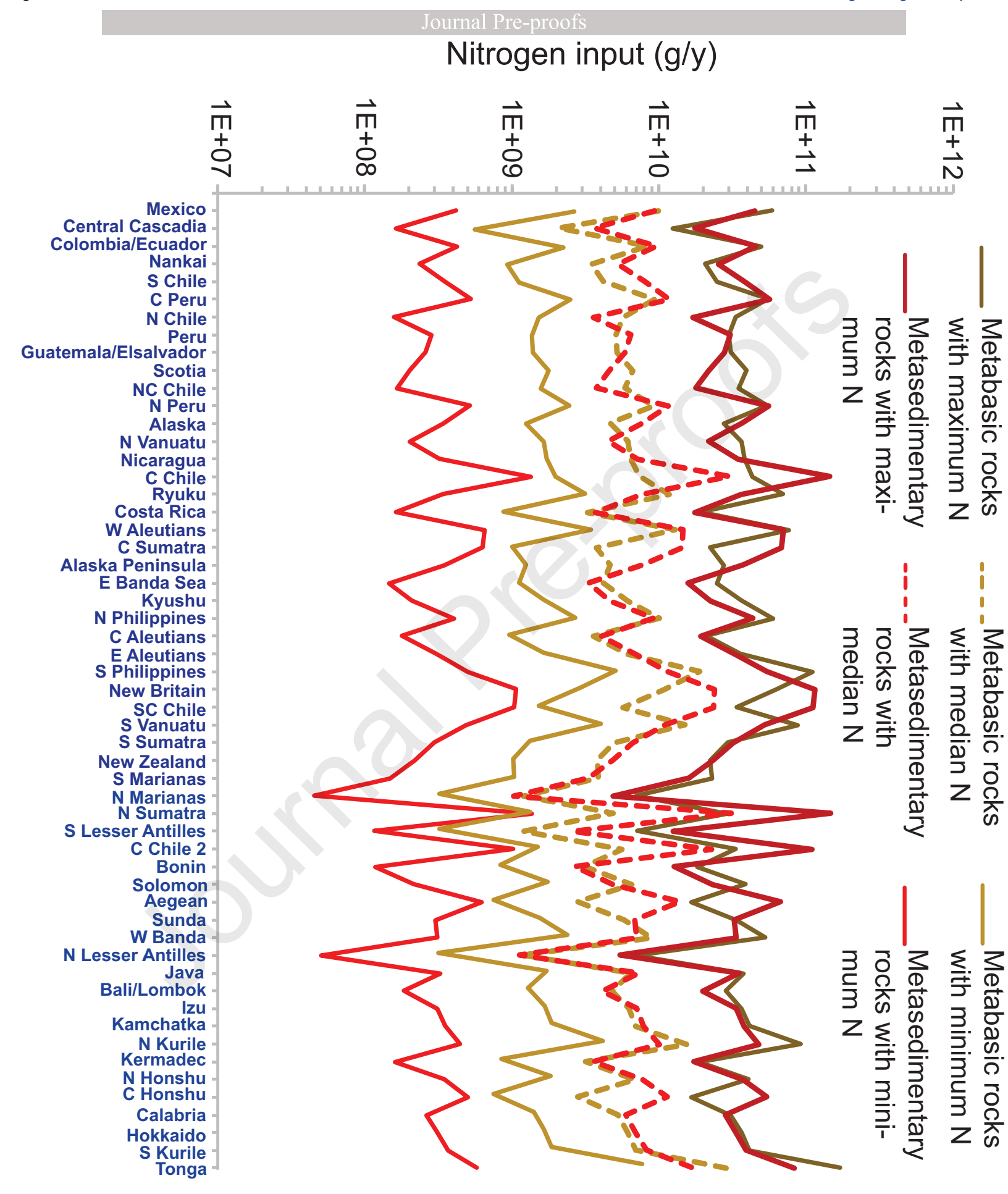
- oceanic crust at ODP Sites 801 and 1149. *Geochemistry, Geophys. Geosystems* **4,** 8910.
- King R. L., Kohn M. J. and Eiler J. M. (2003) Constraints on the petrologic structure of the subduction zone slab-mantle interface from Franciscan Complex exotic ultramafic blocks. *GSA Bull.* **115**, 1097–1109.
- Li C., R. C., Hu K., Yu Z. and H. Y. (1995) Study on the Paleo-Tethys Suture Zone of Lungmu Co-Shuanghu, Tibet. *Geol. Publ. House, Beijing, China.*
- Li K., Li G.-Y., Du Y.-F., Han W., Zhang J., Chen L.-H., Zhou J.-B. and Li L. (2021) Intraslab remobilization of nitrogen during early subduction facilitates deep nitrogen recycling: Insights from the blueschists in the Heilongjiang Complex in NE China. *Chem. Geol.* **583**, 120474.
- Li K. and Li L. (2023a) Alteration enrichment of nitrogen in the gabbroic oceanic crust: Implications for global subducting nitrogen budget and subduction-zone nitrogen recycling. *Geochim. Cosmochim. Acta* **351**, 96–107.
- Li K. and Li L. (2023b) Nitrogen enrichment in the altered upper oceanic crust: A new perspective on constraining the global subducting nitrogen budget and implications for subduction-zone nitrogen recycling. *Earth Planet. Sci. Lett.* **602**, 117960.
- Li K. and Li L. (2022) Nitrogen enrichments in sheeted dikes and gabbros from DSDP/ODP/IODP Hole 504B and 1256D: Insights into nitrogen recycling in Central America and global subduction zones. *Geochim. Cosmochim. Acta* **335**, 197–210.
- Li L., Bebout G. E. and Idleman B. D. (2007) Nitrogen concentration and δ15N of altered oceanic crust obtained on ODP Legs 129 and 185: Insights into alteration-related nitrogen enrichment and the nitrogen subduction budget. *Geochim. Cosmochim. Acta* **71**, 2344–2360.
- Li L., He Y., Zhang Z. and Liu Y. (2021a) Nitrogen isotope fractionations among gaseous and aqueous NH4+, NH3, N2, and metal-ammine complexes: Theoretical calculations and applications. *Geochim. Cosmochim. Acta* **295**, 80–97.
- Li L., Li K., Li Y., Zhang J., Du Y. and Labbe M. (2021b) Recommendations for offline combustion-based nitrogen isotopic analysis of silicate minerals and rocks. *Rapid Commun. Mass Spectrom.* **35**, e9075.
- Liang X., Wang G., Yang B., Ran H., Zheng Y., Du J. and Li L. (2017) Stepwise exhumation of the triassic lanling high-pressure metamorphic belt in central Qiangtang, Tibet: Insights from a coupled study of metamorphism, deformation, and geochronology. *Tectonics* **36**, 652–670.
- Liu Y., Li C., Xie C., Wang M. and Fan J. (2017) Geochronology of the Duguer range metamorphic rocks, Central Tibet: implications for the changing tectonic setting of the South Qiangtang subterrane. *Int. Geol. Rev.* **59**, 29–44.

- Mallik A., Li Y. and Wiedenbeck M. (2018) Nitrogen evolution within the Earth's atmosphere—mantle system assessed by recycling in subduction zones. *Earth Planet. Sci. Lett.* **482**, 556–566.
- Plank T. and Langmuir C. H. (1998) The chemical composition of subducting sediment and its consequences for the crust and mantle. *Chem. Geol.* **145**, 325–394.
- Pullen A., Kapp P., Gehrels G. E., Vervoort J. D. and Ding L. (2008) Triassic continental subduction in central Tibet and Mediterranean-style closure of the Paleo-Tethys Ocean. *Geology* **36**, 351–354.
- Sadofsky S. J. and Bebout G. E. (2003) Record of forearc devolatilization in low-T, high-P/T metasedimentary suites: Significance for models of convergent margin chemical cycling. *Geochemistry, Geophys. Geosystems* **4**, Q03I15.
- Scholl D. W. and Von Huene R. (2007) Crustal recycling at modern subduction zones applied to the past-issues of growth and preservation of continental basement crust, mantle geochemistry, and supercontinent reconstruction. In *Memoir of the Geological Society of America* (eds. R. D. Hatcher Jr., M. P. Carlson, J. H. McBride, and J. R. M. Catalán). Geological Society of America. pp. 9–32.
- Seyfried W. E., Chen X. and Chan L. H. (1998) Trace element mobility and lithium isotope exchange during hydrothermal alteration of seafloor weathered basalt: an experimental study at 350°C, 500 bars. *Geochim. Cosmochim. Acta* **62**, 949–960.
- Shannon R. D. (1976) Revised effective ionic radii and systematic studies of interatomic distances in halides and chalcogenides. *Acta Crystallogr. Sect. A* **32**, 751–767.
- Sidey V. (2016) On the effective ionic radii for ammonium. *Acta Crystallogr. Sect. B Struct. Sci. Cryst. Eng. Mater.* **72**, 626–633.
- Sorensen S. S., Grossman J. N. and Perfit M. R. (1997) Phengite-hosted LILE enrichment in eclogite and related rocks: Implications for fluid-mediated mass transfer in subduction zones and arc magma genesis. *J. Petrol.* **38**, 3–34.
- van der Straaten F., Halama R., John T., Schenk V., Hauff F. and Andersen N. (2012) Tracing the effects of high-pressure metasomatic fluids and seawater alteration in blueschist-facies overprinted eclogites: Implications for subduction channel processes. *Chem. Geol.* **292–293**, 69–87.
- Sun S. S. and McDonough W. F. (1989) Chemical and isotopic systematics of oceanic basalts: Implications for mantle composition and processes. *Geol. Soc. Spec. Publ.* **42**, 313–345.
- Syracuse E. M., van Keken P. E. and Abers G. A. (2010) The global range of subduction zone thermal models. *Phys. Earth Planet. Inter.* **183**, 73–90.
- Tang X. C. and Zhang K. J. (2014) Lawsonite- and glaucophane-bearing blueschists

- from NW Qiangtang, northern Tibet, China: Mineralogy, geochemistry, geochronology, and tectonic implications. *Int. Geol. Rev.* **56**, 150–166.
- Tian Y., Liang X., Wang G., Tang Y., Chen S., Gao X., Yang B., Guo Z., Wang Y. and Wen J. (2023) Protolith origin of the Lanling high-pressure metamorphic terrane in central Qiangtang, Tibet, reveals the subduction of the Permian–Triassic ocean island and abyssal submarine fan in the Paleo-Tethys Ocean. *Gondwana Res.* **121**, 404–417.
- Wu H., Li C., Chen J. and Xie C. (2016) Late Triassic tectonic framework and evolution of Central Qiangtang, Tibet, SW China. *Lithosphere* **8**, 141–149.
- Xu W., Liu F., Zhai Q. and Dong Y. (2021) Petrology and P–T path of blueschists from central Qiangtang, Tibet: Implications for the East Paleo-Tethyan evolution. *Gondwana Res.* **94**, 12–27.
- Zhai Q. G., Jahn B. M., Zhang R. Y., Wang J. and Su L. (2011) Triassic Subduction of the Paleo-Tethys in northern Tibet, China: Evidence from the geochemical and isotopic characteristics of eclogites and blueschists of the Qiangtang Block. *J. Asian Earth Sci.* 42, 1356–1370.
- Zhang K. J., Cai J. X., Zhang Y. X. and Zhao T. P. (2006) Eclogites from central Qiangtang, northern Tibet (China) and tectonic implications. *Earth Planet. Sci. Lett.* **245**, 722–729.
- Zhang X., Dong Y., Li C., Xie C., Wang M., Deng M. and Zhang L. (2014) A record of complex histories from oceanic lithosphere subduction to continental subduction and collision: Constraints on geochemistry of eclogite and blueschist in Central Qiangtang, Tibetan Plateau. *Acta Petrol. Sin.* **30**, 2821–2834.
- Zhang X. Z., Dong Y. S., Wang Q., Dan W., Zhang C., Xu W. and Huang M. L. (2017) Metamorphic records for subduction erosion and subsequent underplating processes revealed by garnet-staurolite-muscovite schists in central Qiangtang, Tibet. *Geochemistry, Geophys. Geosystems* **18**, 266–279.







Declaration of interests	
☑ The authors declare that they have no known competing financial interests or personal relationships that could have appeared to influence the work reported in this paper.	
□The authors declare the following financial interests/personal relationships which may be considered as potential competing interests:	